Modelling of wear defects under anti vibration bars in U-bend for the Eddy Current inspection of Steam Generator tube

Audrey Vigneron, Edouard Demaldent, Jean-Marc Decitre, Thierry Sollier

e-Journal of Nondestructive Testing - ISSN 1435-4934 - www.ndt.net

JOURNEES COFREND 2023 – Marseille du 6 au 8 juin / June 6th to 8th

Modelling of wear defects under Anti Vibration Bars in U-bend for the Eddy Current inspection of Steam Generator tube

Audrey Vigneron[1], Edouard Demaldent[1], Jean-Marc Decitre[2], Thierry Sollier[2]

[1] Université Paris-Saclay, CEA LIST, France

[2]IRSN, France

*corresponding author, E-mail: audey.vigneron@cea.fr

Abstract

The purpose of the anti-vibration bars (AVBs) positioned on both sides of the U-bend part of the steam generator tubes is to limit the vibratory phenomena. These tubes are prone to localized rubbing against the AVBs, resulting in friction-induced wear. To address this issue, eddy current (EC) monitoring and analysis tools like simulation are developed [1]. The objective of the joint study conducted by CEA LIST and IRSN, is to simulate the wear signal under the AVB and to assess the influence of the main geometric parameters on this signal. Within this context, new advanced geometric tools, such as the vibratory movement of an object have been developed to enhance the CIVA model developed at CEA LIST, [2][3]. This 3D numerical model has been experimentally validated on simple configurations involving a machined tube with rectangular-bottomed flats and an AVB, inspected by two axial bobbin coils. The obtained results demonstrate that the presence of AVBs significantly influences the signature of defects near them, especially for thin defect.

1. Introduction

Steam generators (SGs) play a crucial role in French PWR (Pressurised Water Reactor) nuclear power plants. These plants typically have three or four SGs housed within the reactor building, consisting of several thousand tubes shaped like an inverted 'U' and measuring around twenty meters in length. The combined surface area of these steam generator tubes is equivalent to the size of a soccer field and carries out the exchange of heat between the primary loop (inside the tubes) and the secondary loop (outside the tubes). Due to their criticality in ensuring nuclear safety, the SG tubes undergo regular non-destructive examinations to detect any indications or defects.

Eddy currents non-destructive testing (ECNDT) techniques are employed to monitor SG tubes, enabling the detection of newly developed indications and the monitoring of changes in pre-existing indications. If the indications identified during an inspection reach critical dimensions that could result in tube rupture or any other safety-related event within the nuclear facility, the affected tube is plugged to maintain the integrity of the barrier between the primary and secondary loops. When necessary, steam generators can be replaced.

The ongoing research conducted by the operator and safety authorities aims to enhance the detection and characterization of defects through ECNDT. In this context, simulation tools are being utilized to assess the effectiveness of existing and upcoming ECNDT techniques.

The U-bend section of steam generator tubes experiences vibratory phenomena, which are mitigated by the presence of anti-vibration bars but can lead to fretting wear. Distinguishing the EC signature of this wear from the signature specific to the AVB can be challenging. Therefore, during ECNDT inspections, it is crucial to identify and detect such indications, as they can potentially lead to tube rupture, as described in [5]. Consequently, the objective of this study is to model the EC signal of a damaged SG tube resulting from frictional wear in the presence of AVBs.

2. Modelling tools

A specific module within the CIVA software has been developed to simulate the ECNDT inspection of SG tubes. This module utilizes a 3D solver based on the boundary element method, as detailed in [2] and [3]. Designed to accommodate non-standard geometries, the SG tube inspection module is capable of handling various external objects such as the AVB and support plates, as depicted in Figure 1. All numerical parameters, including the mesh, are automatically managed by the module.

 https://doi.org/10.58286/28500

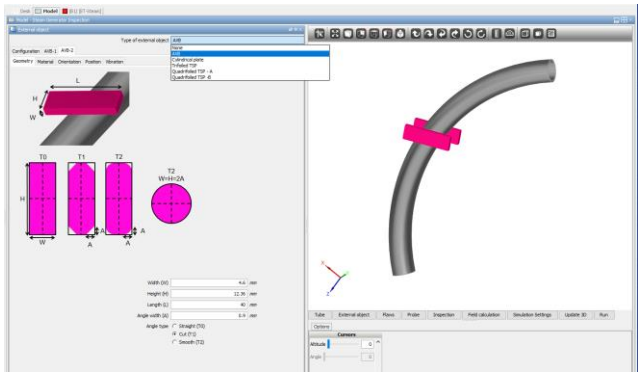

Figure 1: Steam Generator Tube Inspection module in CIVA software.

The SG tubes inspection module is specifically designed for the inspection of steam generator tubes and includes a catalog of industrial probes. These probes have predefined and simplified parameters, encompassing the various components of the probe and optimized trajectory control through the definition of a probe body. Additionally, small variations between elements have been incorporated to account for manufacturing irregularities that may occur.

To model a wear under external objects, the defect is generated by introducing a variation in the position of the object to represent its vibratory movements. This variation is described using an ellipsoidal representation, where an amplitude of movement is defined in each Cartesian direction. These positional variations are stored as a collection of object positions. The defect itself is modeled by locally reducing the radius of the outer wall of the tube at any point where it intersects with the object's surface, ensuring contact is made only at the surface, as shown in Figure 2 (a) and (b). This process is repeated for each representative position of the vibration, as illustrated in Figure 2 (c). Finally, a smoothing process is applied to ensure a precise geometric representation of the defect by the mesh (made of high-order curved boundary elements), even if the edges of the mesh do not precisely follow the shape of the wear defect. This smoothing process helps prevent interpolation errors, as demonstrated in Figure 3. It is important to note that the accuracy of the calculation is not compromised by the smoothing process, as the artificial geometric variation remains within the range of mesh accuracy.

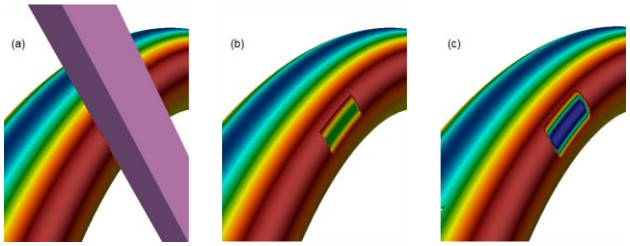

Figure 2: Modelling of a friction wear defect on the outer wall of the SG tube: positioning of the outer object (a), updating of the radius map of the outer wall to offset the re-entrant points (b), repetition for a list of positions representative of the vibration of the outer object (c).

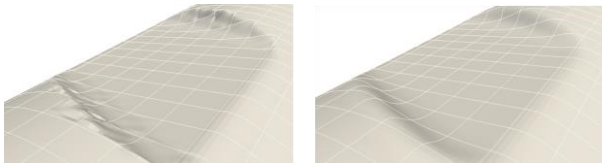

Figure 3: Representation of the geometry interpolated by the calculation mesh before (left) and after (right) applying the smoothing process.

3. Experimental validations

3.1. Experimental setup

Experimental acquisitions are conducted using an axial probe composed of two identical bobbin coils spaced 1 mm apart. The coils have an internal radius of 14 mm, an external radius of 14.8 mm, a height of 2 mm, and consist of 40 turns.

To facilitate the movement of the probe, a puller/pusher system is employed, and the resulting EC signals are acquired using an impedance-meter. A dedicated test bench securely holds the tubes to be inspected and positions a representative sample of an anti-vibration bar. The AVB is constructed from Inconel 600, as depicted in Figure 4, with the specific dimensions provided in Figure 5. The position of the AVB in relation to the tube is adjustable: a micrometric table enables precise adjustment of the distance between the sample and the external wall of the tube, while a rotating table allows for angular placement of the AVB with respect to the tube's axis, as illustrated in Figure 6.

Figure 4: Representative sample of an AVB in Inconel 600.

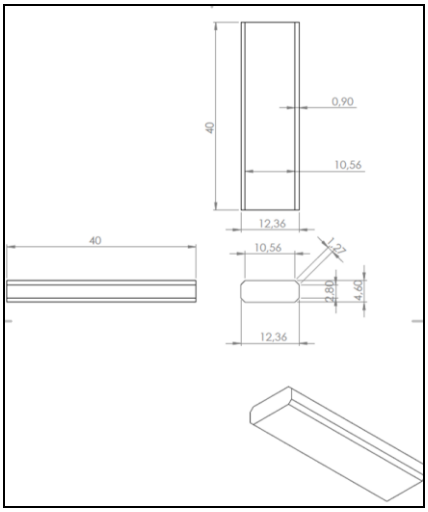

Figure 5: Dimensions of the AVB sample.

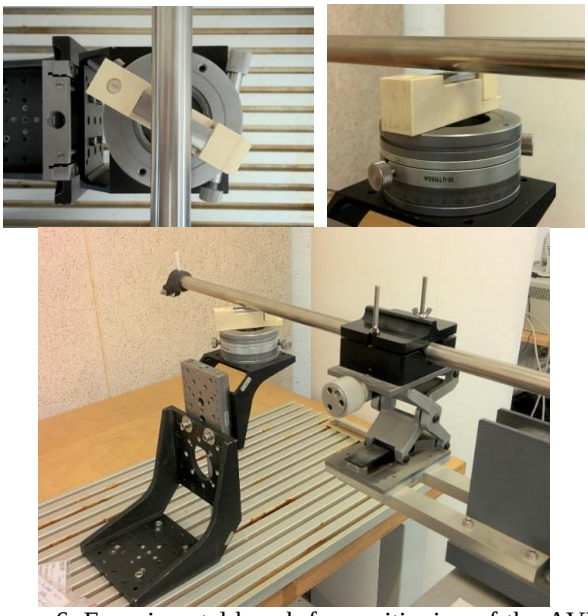
Figure 6. Experimental bench for positioning of the AVB near to the tube inspected.

Two samples from the same Inconel 690 TT SG tube are employed in the study. The first sample consists of a tube with straight wear, featuring machined rectangular bottoms and varying depths ranging from 20% to 60% of the tube thickness. The second sample is specifically designed for calibrating industrial nuclear probes. The dimensions of the defects present in the samples are detailed in Table 1 and Table 2.

Table 1: Straigth wears.

Label	Dimensions
SW20	Straight wear with rectangular bottom 20%
SW30	Straight wear with rectangular bottom 30%
SW40	Straight wear with rectangular bottom 40%
SW60	Straight wear with rectangular bottom 60%

Table 2 : Calibration defects.

Label	Dimensions
4Ø1	4 through wall Φ1 holes, spaced by 90°
LEG30	Large External circumferential Groove 30% width 20 mm
EG40	External circumferential Groove 40% width 1 mm
IG10	Internal circumferential Groove 10 % width 1 mm

3.2. Validations expérimentales

All the results presented below are acquired at 280 kHz in differential mode and calibrated using the 4Ø1 unless otherwise specified.

The comparison between simulation and experimental acquisition for the calibration defects is depicted in Figure 7, while Figure 8 illustrates the comparison for the straight wears. Notably, the results demonstrate a high level of accuracy between the simulation and experimental data.

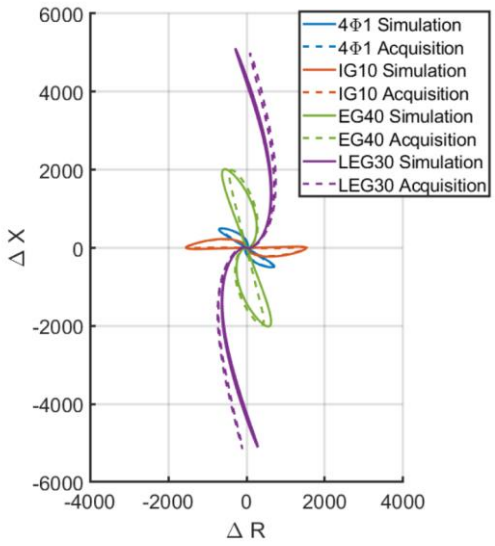

Figure 7: Experimental comparison for calibration defects at 280 kHz.

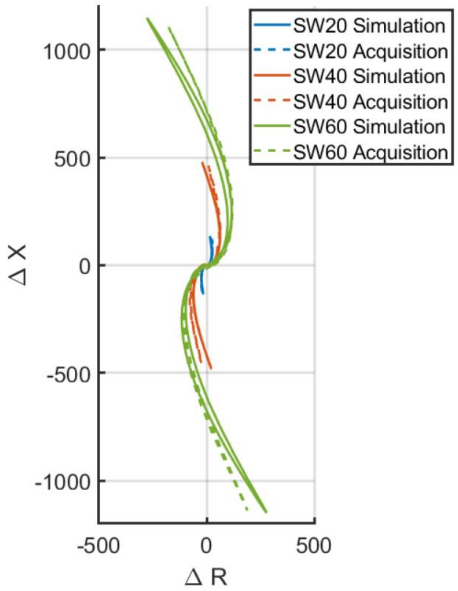

Figure 8: Experimental comparison for straight wears at 280 kHz.

Table 3 and
Table 4 present the EC signal amplitude and phase values for both the experimental acquisitions and simulations. The difference between the model and the acquisitions is approximately 4% in amplitude and 4° in phase. Notably, there is a strong agreement for the IG10, which represents an internal groove, despite the signals being calibrated on the four through holes, which can be considered as internal faults. The Table 5 and Table 6 display the same results but with calibration on an external fault, specifically the 40% external groove. As expected, we observe a reversal in the trend, with a difference of around 4% in amplitude and 4° in phase between experimental acquisitions and simulations for internal defects. However, there is an excellent agreement for external defects.

These results serve to validate the model for standard defects and straight wear with rectangular bottom. The residual deviation of approximately 4% and 4°, consistent across different models, requires further investigation. It is likely attributed to a parameter within the experimental setup that has not been considered in the simulations.

Table 3 : Experimental comparison for the EC signal amplitude at 280 kHz, with the 4Ø1 calibration.

Defect label	Acquisition (mV)	Simulation (mV)	Difference (%)
4Ø1	**1700.00**	**1700.00**	**0.00**
LEG30	10155.07	10231.03	0.74
EG40	4044.12	4188.63	3.45
IG10	3096.02	3056.09	1.31
SW20	254.22	267.02	4.80
SW40	918.27	961.92	4.54
SW60	2276.01	2363.20	3.69

Table 4: Experimental comparison for the EC signal phase at 280 kHz, with the 4Ø1 calibration.

Defect label	Acquisition (°)	Simulation (°)	Difference (°)
4Ø1	**-35.00**	**-35.00**	**0.00**
LEG30	-91.08	-86.75	4.33
EG40	-78.66	-74.09	4.57
IG10	-0.13	-0.20	0.07
SW20	-100.91	-97.00	3.91
SW40	-92.17	-87.40	4.77
SW60	-80.77	-76.44	4.33

Table 5: Experimental comparison for the EC signal amplitude at 280 kHz, with the external calibration.

Defect label	Acquisition (mV)	Simulation (mV)	Difference (%)
4Ø1	1760.75	1700.00	3.57
LEG30	10517.94	10231.03	2.80
EG40	**4188.63**	**4188.63**	**0.00**
GI10	3206.65	3056.09	4.93
SW20	263.30	267.02	1.39
SW40	951.08	961.92	1.13
SW60	2357.34	2363.20	0.25

Table 6: Experimental comparison for the EC signal phase at 280 kHz, with the external calibration.

Defect label	Acquisition (°)	Simulation (°)	Difference (°)
4Ø1	-30.43	-35.00	4.57
LEG30	-86.51	-86.75	0.24
EG40	**-74.09**	**-74.09**	**0.00**
GI10	4.44	-0.20	4.64
SW20	-96.34	-97.00	0.66
SW40	-87.60	-87.40	0.20
SW60	-76.20	-76.44	0.24

Next, we investigate a straight wear with rectangular bottom with a depth of 20% and an Inconel AVB positioned at a 90° angle to the tube axis. The BAV is located at distances of 0.0 mm, 0.2 mm, and -0.2 mm from the outer surface (without defect) of the tube. Negative positions indicate the AVB nearing the bottom of the defect, while positive values indicate the AVB moving away from it. Please refer to Figure 9 for visual reference.

Figure 10 exhibits a strong agreement between the simulated and acquired signals, the amplitude difference between the model and experimental acquisitions ranging from 6% to 9%, and a phase difference of 6° to 8% when calibrated on the through holes. Similarly, as observed in previous comparisons, Table 7 and Table 8 indicate a reduced difference when calibrated on an external defect, specifically the EG40.

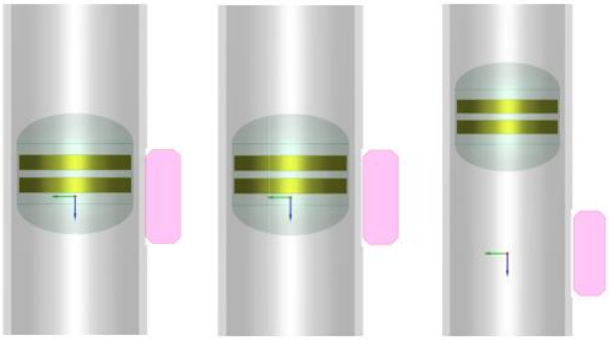

Figure 9: The AVB is placed at 90° angle to the tube axis and -0.2 mm (left), 0 mm (center) and 0.2 mm (right) on the outer wall of the tube.

Table 7: Experimental comparison for the EC signal amplitude at 280 kHz, with the external calibration.

Defect label	AVB position (mm)	Acquisition (°)	Simulation (°)	Difference (°)
4Ø1	-	1760.75	1700.00	3.57
EG40	**-**	**4188.63**	**4188.63**	**0.00**
SW20	-0.2	230.15	244.78	5.98
SW40	0.0	206.52	215.68	4.25
SW60	0.2	200.35	205.34	2.43

Table 8: Experimental comparison for the EC signal phase at 280 kHz, with the external calibration.

Defect label	AVB position (mm)	Acquisition (°)	Simulation (°)	Difference (°)
4Ø1	-	-30.43	-35.00	4.57
EG40	**-**	**-74.09**	**-74.09**	**0.00**
SW20	-0.2	-6.63	-4.79	1.84
SW40	0.0	-23.02	-19.46	3.56
SW60	0.2	-38.51	-34.82	3.69

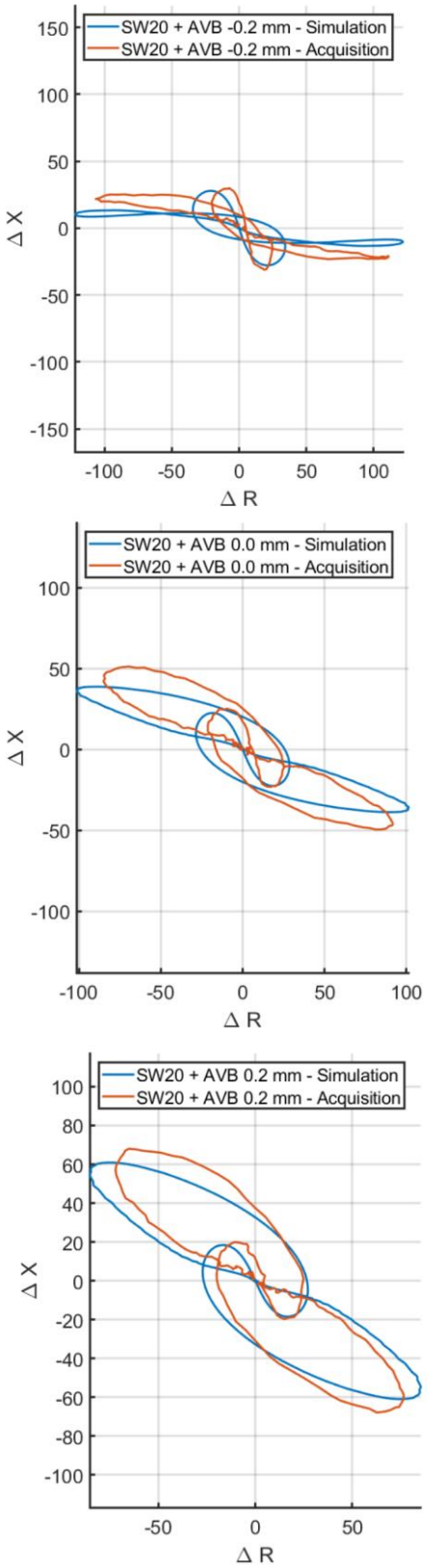

Figure 10: Experimental comparison for straight wear and AVB placed at different distance from the external tube wall, the calibration defect is the 4Ø1.

4. Conclusions

The exploitation of modeling tools for eddy current testing of U-bend steam generator tubes in the presence of anti-vibration bars and associated friction wear has been presented in this document. These tools are available in the commercial software CIVA and have been experimentally validated.

The modeling tools provided by CEA enable IRSN to conduct parametric studies for evaluating the detection and characterization performance of defects in steam generator tubes.

References

[1] L. Maurice, V. Costan and P. Thomas, “Axial probe eddy current inspection of steam generator tubes near anti-vibration bars: performance evaluation using finite element modeling,” in Proceedings of JRC-NDE, Cannes, 2013.

[2] M. Bonnet and E. Demaldent, “The eddy current model as a low-frequency, high-conductivity asymptotic form of the Maxwell transmission problem,” in Computers & Mathematics with Applications, vol. 77, n°18, 2019.

[3] M. Bonnet and E. Demaldent, “Eddy-current asymptotics of the Maxwell PMCHWT formulation for multiple bodies and conductivity levels,” in Computers & Mathematics with Applications, vol. 141, 2023.

[4] A. Vigneron, E. Demaldent, F. Nozais and T. Sollier, “Modelling of wear defects under Anti Vibration Bars in U-bend,” in NDE in Nuclear, Charlotte, 2019.

[5] W. Cheng and I. Finnie, “Stress analysis and fatigue life prediction for a U-bend steam generator tube,” Nuclear Engineering and Design, vol. 165, pp. 101-109, 1996.